AIP | Applied Physics Letters

Second harmonic detection in the electrochemical strain microscopy of Ag-ion conducting glass

Sang Mo Yang, M. Baris Okatan, M. Parans Paranthaman, Stephen Jesse, Tae Won Noh, and Sergei V. Kalinin

Citation: Applied Physics Letters **105**, 193106 (2014); doi: 10.1063/1.4901736
View online: http://dx.doi.org/10.1063/1.4901736
View Table of Contents: http://scitation.aip.org/content/aip/journal/apl/105/19?ver=pdfcov
Published by the AIP Publishing

Second harmonic detection in the electrochemical strain microscopy of Ag-ion conducting glass

Sang Mo Yang,[1,2,3,a)] M. Baris Okatan,[3] M. Parans Paranthaman,[4] Stephen Jesse,[3] Tae Won Noh,[1,2] and Sergei V. Kalinin[3]
[1]*Center for Correlated Electron Systems, Institute for Basic Science (IBS), Seoul 151-742, South Korea*
[2]*Department of Physics and Astronomy, Seoul National University, Seoul 151-742, South Korea*
[3]*Center for Nanophase Materials Sciences, Oak Ridge National Laboratory, Oak Ridge, Tennessee 37831, USA*
[4]*Chemical Sciences Division, Oak Ridge National Laboratory, Oak Ridge, Tennessee 37831, USA*

(Received 14 August 2014; accepted 3 November 2014; published online 14 November 2014)

The first and second harmonic electromechanical responses and their cross-correlation in Ag-ion conducting glass were investigated using band-excitation electrochemical strain microscopy (ESM). Consecutive ESM images with increasing magnitudes of the applied AC voltage allowed observation of not only reversible surface displacement but also irreversible silver nanoparticle formation above a certain threshold voltage. The second harmonic ESM response was anti-correlated with the first harmonic response in many local regions. Furthermore, the nucleation sites of silver nanoparticles were closely related to the anti-correlated regions, specifically, with low second harmonic and high first harmonic ESM responses. The possible origins of the second harmonic ESM response are discussed. © *2014 AIP Publishing LLC*. [http://dx.doi.org/10.1063/1.4901736]

Electrochemical strain microscopy (ESM) has recently emerged as a powerful tool to probe ionic transport and electrochemical phenomena at the nanoscale in many material systems, ranging from Li ion systems[1–3] to oxide electrolytes[4] and memristive materials.[5] ESM is based on the detection of electrochemical strains generated in solids in response to a periodic bias applied to the tip.[1,2] This technique is similar to the well-established piezoresponse force microscopy,[6–8] with the primary difference lying in the signal generation mechanism.

The origins of electrochemical strain can include Vegard strain,[9,10] the electrostrictive response of materials to induced chemical polarization and surface electrochemical reactions, as well as multiple other mechanisms.[11–13] In the Vegard case, the induced strain is linearly proportional to the concentration change of mobile species, generated by the electrochemical process at the tip-surface junction. Alternatively, the formation of electrochemical double layers or surface charges (consequently creating chemical or physical polarization) coupled with bulk electrostriction can produce hysteretic first harmonic responses.[14–16] Further insight into the mechanisms of ESM can be obtained by the observation of second harmonic responses related to electrostriction or reversible ionic motion. Here, we explored the first and second harmonic ESM responses and their cross-correlation in Ag-ion conducting glass.

As a model system for higher-order harmonic ESM detection, we chose a $(AgI)_{0.2}(AgPO_3)_{0.8}$ glass (~3.0 mm thick). $(AgI)_x(AgPO_3)_{1-x}$ glass is one of the well-known solid electrolytes with mobile Ag^+ ions, and its conductivity is high (e.g., 10^{-2} Scm^{-1} at $x = 0.6$).[17] Additionally, Ag-ion conducting glass is stable in air, compared with other solid electrolytes, such as Li-ion systems. The sample was prepared by a melt-quenching method.[18–22] Stoichiometric quantities of reagent-grade starting chemicals, ammonium dihydrogen phosphate ($NH_4H_2PO_4$), silver nitrate ($AgNO_3$), and silver iodide (AgI), were weighed, ground, and heated in an alumina crucible placed in a box furnace at 300 °C for 1 h and finally heat-treated at 700 °C for 1 h in air. The melt was then quenched by pressing between two stainless steel plates to prepare $(AgI)_{0.2}(AgPO_3)_{0.8}$ glass.[18–22]

To measure the spatial maps of higher-order harmonic ESM responses at the sub-10 nm scale, we used band-excitation (BE)-ESM.[23] Briefly, an electric bias with a band of frequencies around the contact resonance of the cantilever was applied, and the response was measured and Fourier-transformed simultaneously to yield the total ESM response. It was then analyzed using a simple harmonic oscillator model fitting to extract signals for amplitude, phase, resonance frequency, and quality factor. Note that the BE approach mitigates significantly the topographic cross-talk by the position-dependent cantilever transfer function.[23] BE-ESM was performed using a commercial atomic force microscope (Cypher, Asylum Research) interfaced with National Instrument cards controlled by Labview and Matlab software. The BE signal, at 350–410 kHz, was applied to the cantilever with a conductive Pt/Cr coating (Budget Sensors). For electrical contact, a silver paste was used as the bottom electrode. Image and data processing were performed using WSxM[24] and custom-written Matlab codes, respectively.

First, we investigated the first harmonic ESM signals of $(AgI)_{0.2}(AgPO_3)_{0.8}$ glass. A topographic image ($5 \times 5\ \mu m^2$) of the glass showed multiple pores and initially existing particles (Fig. 1(a)). Figures 1(b) and 1(c) show the spatial maps of the first harmonic BE-ESM amplitude and resonance frequency obtained by a simple harmonic model fitting, respectively. The magnitude of the applied AC voltage (V_{ac}) for ESM imaging was 3 V. The amplitude signal was high at the boundary of the top largest pore, but it was remarkably low in other regions. The resonance frequency signal showed

a)Electronic mail: yangs@ornl.gov

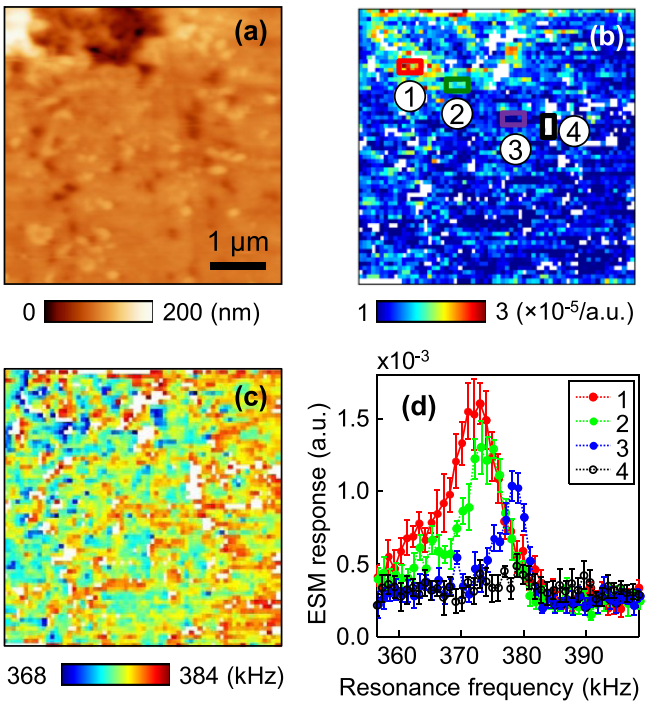

FIG. 1. (a) Topographic image of $(AgI)_{0.2}(AgPO_3)_{0.8}$ glass. Spatial maps of the first harmonic BE-ESM (b) amplitude and (c) resonance frequency analyzed using a simple harmonic oscillator model fitting. The applied AC voltage for BE-ESM imaging was 3 V. All image sizes are $5 \times 5\ \mu m^2$. (d) ESM responses were averaged at the four different regions marked in (b). Note that the maximum peak values at the resonance frequency are those obtained by multiplying the amplitude and quality factor.

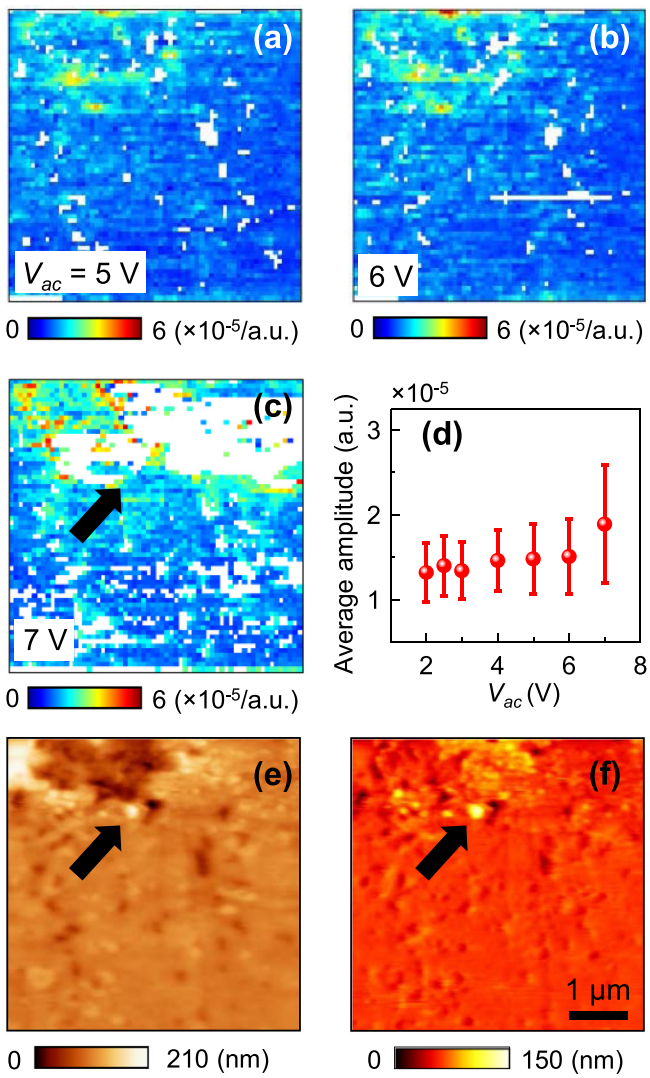

FIG. 2. ESM amplitude images at the different V_{ac}: (a) 5 V, (b) 6 V, and (c) 7 V. (d) The amplitude values averaged over all pixels (except the white pixels) as a function of V_{ac}. The error bars indicate the standard deviations. (e) Topographic image after ESM imaging with $V_{ac} = 7$ V, showing the formation of silver metal nanoparticles. (f) Difference image made from the subtraction between the topographic images before (Fig. 1(a)) and after the formation of silver particles (Fig. 2(e)). Bright (yellow) regions show the silver nanoparticles formed. All image sizes are $5 \times 5\ \mu m^2$.

variation (~15 kHz), likely due to changes in the contact stiffness depending on the position (i.e., pores and particles). White pixels in these images represent the points where the ESM response was close to zero (Fig. 1(d)), and thus were not amenable to fitting.

Using consecutive ESM images with increasing V_{ac}, we observed not only reversible surface displacement but also an irreversible electrochemical reaction above a certain threshold voltage (Figs. 2(a)–2(c)). Until the V_{ac} reached 6 V, the local ESM amplitude increased slightly with V_{ac}, but topographic images and the resonance frequency maps did not show any change (see Ref. 25). The average value of the ESM amplitude for all pixels (except the white pixels) also showed a slight increase (Fig. 2(d)). This indicated that the applied AC bias yielded only a reversible change in surface displacement. However, at $V_{ac} = 7$ V, many nanoparticles were formed suddenly, as indicated by the arrows in Figs. 2(e) and 2(f). The nanoparticle nucleation sites coincided with the high ESM amplitude regions (i.e., the vicinity of the top largest pore). The average value of the ESM amplitude also increased markedly. The newly formed nanoparticles should be silver metal particles. That is, an irreversible electrochemical Ag reduction process occurred when critical potential was exceeded: $Ag^+ + e^- \rightarrow Ag(s)$. The observed threshold voltage is considerably larger than the thermodynamically determined standard Ag reduction potential (~0.8 V). However, the Ag reduction reaction is a kinetic process, driven by the applied AC bias with high frequency ω. Thus, the condition of $\omega\tau \sim 1$ should be fulfilled under AC bias application,[26] where $\tau(V_{ac})$ is the time scale to occur for Ag nucleation. The high bias is required at high frequency AC bias, since τ becomes smaller with increasing the bias (It is expected to decrease to thermodynamic potential, if DC bias is applied.) Furthermore, it should be considered that the overall voltage drop is divided between the tip-surface junction and the bulk material.[4] Thus, the actual voltage driving the formation of silver particles at the tip-surface junction is significantly smaller than the tip bias.

The first harmonic ESM response allows identification of the Ag^+ ion abundant sites. To emphasize the nucleation sites of silver particles, a difference image is presented in Fig. 2(f), prepared by the subtraction between the topographic images before (Fig. 1(a)) and after the formation of silver particles (Fig. 2(e)). The nucleation sites correspond to the region of white pixels in Fig. 2(c), indicating that reversible surface displacement no longer takes place after the nucleation of the silver particles. The sizes of the particles deposited in the higher amplitude regions were larger than

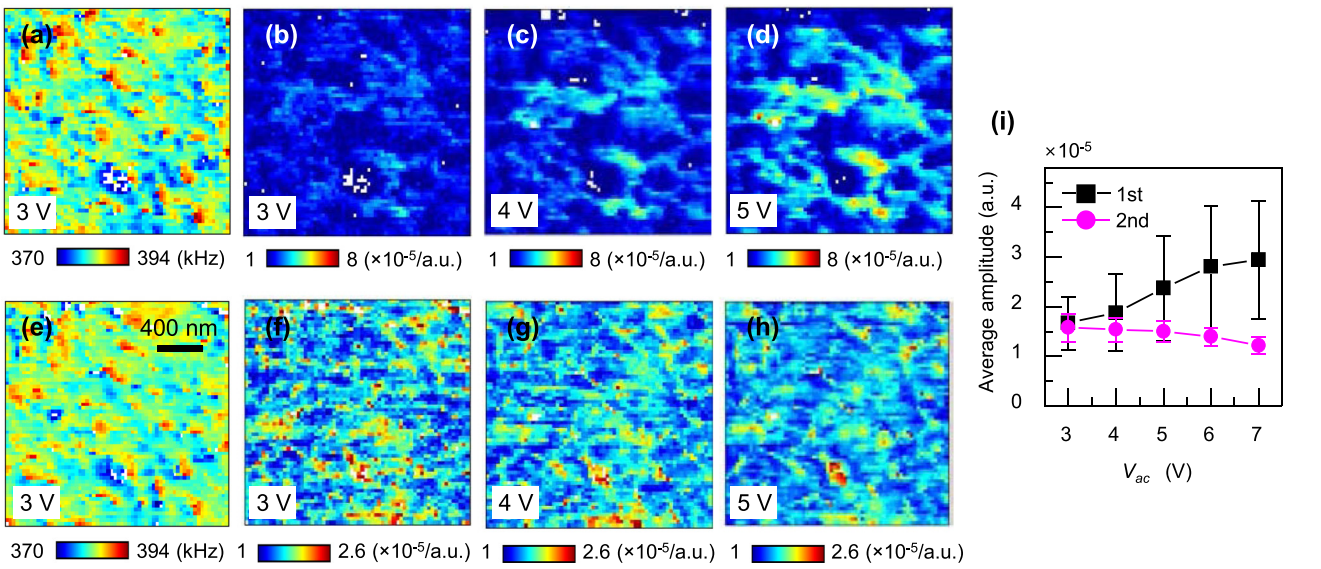

FIG. 3. (a) and (e) Resonance frequency at $V_{ac} = 3$ V and ((b)–(d) and (f)–(h)) V_{ac}-dependent amplitude images for ((a)–(d)) the first harmonic and ((e)–(h)) second harmonic ESM responses, respectively. All image sizes are $2 \times 2\ \mu m^2$. (i) The values of amplitude averaged over all pixels (except the white pixels) as a function of V_{ac} for the first (squares) and second (circles) harmonic ESM responses. The error bars indicate the standard deviations.

those in the lower amplitude regions. This demonstrated that the first harmonic ESM amplitude is directly linked to the concentration of Ag^+ ions.

To gain further insight into the underlying mechanism of ESM, we measured the first and second harmonic responses at the same sample position as a function of V_{ac}. To detect the nth harmonic ($n = 1, 2, \ldots$), we applied a band of frequencies at ω_0/n, where ω_0 is the contact resonance, but still measured the ESM response at ω_0.[27,28] Thus, if the position-dependent contact stiffness (or contact area) does not change during measurement, the resonance frequency images for the nth harmonics should be the same. As shown in Figs. 3(a) and 3(e), the resonance frequency images for the first and second harmonic ESM signals were almost identical. This validates the reliability of our ESM data for the high-order harmonic responses. Third harmonic signals were not detected in this system.

While the resonance frequency images were virtually identical, the amplitude images clearly showed complementary information and evolved differently with V_{ac}. In the spatial maps of the first harmonic ESM amplitude signal, the local amplitude increased from the center to the periphery of the ESM-activated regions (i.e., higher amplitude regions) with V_{ac} (Figs. 3(b)–3(d)). In contrast, in the spatial maps of the second harmonic, the local amplitude decreased slightly from the periphery of the ESM-activated regions with increasing V_{ac}, and consequently, the ESM-activated regions decreased (Figs. 3(f)–3(h)). The V_{ac}-dependent average amplitude showed these increasing and decreasing behaviors for the first and second harmonic responses, respectively (Fig. 3(i)).

To explore this behavior further, we analyzed the cross-correlation between the spatial maps of the first and second harmonic responses. Figures 4(a) and 4(b) show the spatial maps of the first and second harmonic amplitude signals at $V_{ac} = 6$ V (i.e., before the formation of silver particles), respectively. We found that the first and second harmonic amplitude images were anti-correlated in many local regions. For example, in the region indicated by open boxes in Figs. 4(a) and 4(b), the first harmonic signal was high, but the second harmonic was low, and *vice versa*. To analyze their correlation quantitatively, we performed cross-correlation coefficient analysis[29] for the images measured at the same V_{ac}. The cross-correlation coefficients for the resonance frequency images were nearly 1 (the squares in Fig. 4(c)), confirming that they were almost identical. However, the cross-correlation coefficients for the amplitude images were approximately

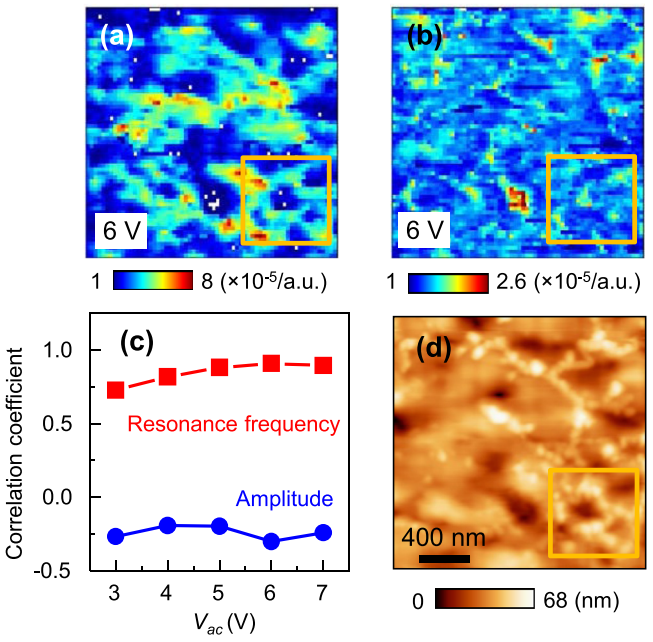

FIG. 4. ESM amplitude images for (a) the first and (b) second harmonics at $V_{ac} = 6$ V. (c) Cross-correlation coefficients between the spatial maps of the first and second harmonic resonance frequency (squares) and amplitude (circles) responses as a function of V_{ac}. (d) Topographic image after ESM imaging with $V_{ac} = 8$ V, showing the formation of silver nanoparticles. All image sizes are $2 \times 2\ \mu m^2$.

−0.25 (the circles in Fig. 4(c)). The negative coefficient value suggests that they are anti-correlated. Furthermore, interestingly, we found that this local anti-correlation was relevant to the occurrence of the surface electrochemical Ag reduction process. Above a certain threshold voltage, silver nanoparticles were formed in the regions (also see Ref. 25) with high first harmonic and low second harmonic amplitude signals, as seen clearly in the open box of Fig. 4(d).

For the mechanism of ESM in this system, we first considered the ionic Vegard strain. The first harmonic ESM response can be explained in terms of the bias-induced Ag-ionic motion and Vegard's law.[9,10] Additionally, the second harmonic response could be generated using the quadratic Coulomb interaction between ions. It has been reported that the induced strain u follows a second-order polynomial of ion concentration change ΔC given by $u \propto a\Delta C - b\Delta C^2$ (where a and b are constants) in a few ion conductors.[30] The first-order term is from Vegard's law, and the second-order term is due to Coulomb interaction between ions. However, for the Vegard mechanism, a reversible electrochemical reaction at the tip-surface junction is required. The Pt/Cr-coated tip is an ion-blocking and electrochemically inert electrode, and a silver reservoir does not exist at the tip-surface junction. Thus, the Ag redox process (i.e., the formation and dissolution of silver nanoparticles) should take place at the tip-surface junction. More investigation to confirm the possibility of a silver nanoparticle dissolution process is needed.

We suggest that surface chemical polarization P_{chem}, coupled with bulk electrostriction, is another possible origin of the ESM response in this system. The formation of an electrochemical double layer (or surface charge layer) on the surface is expected. For example, it can be formed by Ag^+ ions in glass and OH^- ions, which are readily available as a result of dissociative water adsorption.[15] The formation of these layers indicates the existence of P_{chem}, capable of generating both the first and second harmonic ESM responses by coupling with electrostriction Q.[16] Namely, the electric field (E)-induced strain $u = Q(P_{chem} + \varepsilon E)^2 = Q({P_{chem}}^2 + 2P_{chem}\varepsilon E + \varepsilon^2 E^2)$, where $\varepsilon = (1 + \chi_e)\varepsilon_0$ is the permittivity, χ_e is the electric susceptibility, and ε_0 is the vacuum permittivity.[25] The first harmonic ESM response is directly linked to the amount of P_{chem} (i.e., the concentration of Ag^+ ions). The second harmonic response indicates how large χ_e is in the local probing region (i.e., how readily the probing region polarizes in response to an applied bias).

This scenario can explain why silver particles nucleate readily in the regions with high first harmonic and low second harmonic ESM responses. If the first harmonic is high and the second harmonic is low (i.e., P_{chem} is large and χ_e is small), Ag^+ ions are abundant and can remain longer. Thus, both the concentration of Ag^+ ions and the time for nucleation are sufficient, allowing silver particles to be formed easily. In contrast, if the first harmonic is small or the second harmonic is high, Ag^+ ions are scarce or leave rapidly, making it difficult to nucleate silver particles. The local anti-correlation can be explained in terms of the number of Ag^+ ions in the local region. The formation of P_{chem} indicates that Ag^+ ions are bound by anions. As a result, if P_{chem} is large, the number of Ag ions to be polarized decreases, and *vice versa*. Alternatively, it could be simply caused by chemical inhomogeneity in the $(AgI)_{0.2}(AgPO_3)_{0.8}$ glass.

In summary, we explored the first and second harmonic BE-ESM responses in an $(AgI)_{0.2}(AgPO_3)_{0.8}$ glass. The first and second harmonic ESM responses evolved differently with V_{ac}, and the second harmonic response was anti-correlated with the first harmonic in many local regions. Interestingly, silver nanoparticles were formed in regions with high first harmonic and low second harmonic ESM responses. We suggest that surface chemical polarization, coupled with bulk electrostriction, is a likely origin of ESM responses in an Ag-ion conducting glass. To clarify the exact origin, more investigation is needed. This work reveals that ESM is a powerful tool to probe electrochemically active regions at the nanoscale in the metal cation conducting glasses composed of multiple materials. In addition, we highlight that the higher-order harmonic detection and the analysis of their cross-correlation can provide deeper insights into the underlying physics of material systems, such as the origin of electromechanical responses in fast ion conductors with mobile cations.

This research was conducted at and partially supported by (M.B.O., S.J., and S.V.K.) the Center for Nanophase Materials Sciences, which is a DOE Office of Science User Facility. Support (S.M.Y. and S.V.K.) was also provided by a DOE Presidential Early Career for Scientists and Engineers. This research was also partially supported (S.M.Y. and T.W.N.) by IBS-R009-D1, Korea. Materials synthesis work (M.P.P.) was sponsored by the Materials Sciences and Engineering Division, Office of Basic Energy Sciences, U.S. Department of Energy. Thanks are due to Dr. Zhonghe Bi for initial help with synthesis and Dr. Miaofang Chi with microscopy work.

[1]N. Balke, S. Jesse, A. N. Morozovska, E. A. Eliseev, D. W. Chung, Y. Kim, L. Adamczyk, R. E. Garcia, N. Dudney, and S. V. Kalinin, Nat. Nanotechnol. **5**, 749 (2010).
[2]S. Jesse, A. Kumar, T. M. Arruda, Y. Kim, S. V. Kalinin, and F. Ciucci, MRS Bull. **37**, 651 (2012).
[3]N. Balke, S. Jesse, Y. Kim, L. Adamczyk, A. Tselev, I. N. Ivanov, N. J. Dudney, and S. V. Kalinin, Nano Lett. **10**, 3420 (2010).
[4]A. Kumar, F. Ciucci, A. N. Morozovska, S. V. Kalinin, and S. Jesse, Nat. Chem. **3**, 707 (2011).
[5]Y. Kim, J. H. Jang, S.-J. Park, S. Jesse, L. Donovan, A. Y. Borisevich, W. Lee, and S. V. Kalinin, Nanotechnology **24**, 085702 (2013).
[6]A. Gruverman, O. Auciello, and H. Tokumoto, Annu. Rev. Mater. Sci. **28**, 101 (1998).
[7]S. V. Kalinin and D. A. Bonnell, Phys. Rev. B **65**, 125408 (2002).
[8]S. M. Yang, J. G. Yoon, and T. W. Noh, Curr. Appl. Phys. **11**, 1111 (2011).
[9]A. N. Morozovska, E. A. Eliseev, and S. V. Kalinin, Appl. Phys. Lett. **96**, 222906 (2010).
[10]A. N. Morozovska, E. A. Eliseev, N. Balke, and S. V. Kalinin, J. Appl. Phys. **108**, 053712 (2010).
[11]A. N. Morozovska, E. A. Eliseev, A. K. Tagantsev, S. L. Bravina, L.-Q. Chen, and S. V. Kalinin, Phys. Rev. B **83**, 195313 (2011).
[12]A. N. Morozovska, E. A. Eliseev, G. S. Svechnikov, and S. V. Kalinin, Phys. Rev. B **84**, 045402 (2011).
[13]S. V. Kalinin and A. N. Morozovska, J. Electroceram. **32**, 51 (2014).
[14]A. Kumar, T. M. Arruda, Y. Kim, I. N. Ivanov, S. Jesse, C. W. Bark, N. C. Bristowe, E. Artacho, P. B. Littlewood, C.-B. Eom, and S. V. Kalinin, ACS Nano **6**, 3841 (2012).
[15]R. Proksch, J. Appl. Phys. **116**, 066804 (2014).
[16]Q. N. Chen, Y. Ou, F. Ma, and J. Li, Appl. Phys. Lett. **104**, 242907 (2014).
[17]M. Mangion and G. P. Johari, Phys. Rev. B **36**, 8845 (1987).

[18]J. P. Malugani, A. Wasniewski, M. Doreau, G. Robert, and A. A. Rikabi, Mater. Res. Bull. **13**, 427 (1978).
[19]S. W. Martin, J. Am. Ceram. Soc. **74**, 1767 (1991).
[20]H. Takahashi, E. Matsubara, and Y. Waseda, J. Mater. Sci. **29**, 2536 (1994).
[21]H. Takahashi, H. Nakanii, and T. Sakuma, Solid State Ionics **176**, 1067 (2005).
[22]H. Takahashi, H. Nakanii, T. Sakuma, and Y. Onoda, Solid State Ionics **179**, 2137 (2008).
[23]S. Jesse and S. V. Kalinin, J. Phys. D: Appl. Phys. **44**, 464006 (2011).
[24]I. Horcas, R. Fernández, J. M. Gómez-Rodríguez, J. Colchero, J. Gómez-Herrero, and A. M. Baro, Rev. Sci. Instrum. **78**, 013705 (2007).
[25]See supplementary material at http://dx.doi.org/10.1063/1.4901736 for additional images and supporting information.
[26]S. M. Yang, J. Y. Jo, T. H. Kim, J. G. Yoon, T. K. Song, H. N. Lee, Z. Marton, S. Park, Y. Jo, and T. W. Noh, Phys. Rev. B **82**, 174125 (2010).
[27]Y. Kim, A. Kumar, A. Tselev, I. I. Kravchenko, H. Han, I. Vrejoiu, W. Lee, D. Hesse, M. Alexe, S. V. Kalinin, and S. Jesse, ACS Nano **5**, 9104 (2011).
[28]R. K. Vasudevan, M. B. Okatan, I. Rajapaksa, Y. Kim, D. Marincel, S. Trolier-McKinstry, S. Jesse, N. Valanoor, and S. V. Kalinin, Sci. Rep. **3**, 2677 (2013).
[29]Y. Kim, E. Strelcov, I. R. Hwang, T. Choi, B. H. Park, S. Jesse, and S. V. Kalinin, Sci. Rep. **3**, 2924 (2013).
[30]I. E. L. Stephens and J. A. Kilner, Solid State Ionics **177**, 669 (2006).